Biofabrication

International Society for Biofabrication

ACCEPTED MANUSCRIPT

Micro/nanofabrication of brittle hydrogels using 3D printed soft ultrafine fiber molds for damage-free demolding

To cite this article before publication: Shang Lv *et al* 2019 *Biofabrication* in press https://doi.org/10.1088/1758-5090/ab57d8

Micro/nanofabrication of brittle hydrogels using 3D printed soft ultrafine fiber molds for damage-free demolding

Shang Lv[1,2], Jing Nie[1,2], Qing Gao[1,2], Chaoqi Xie[1,2], Luyu Zhou[1,2], Jingjiang Qiu[3], Jianzhong Fu[1,2], Xin Zhao[4], and Yong He*[,1,2,5]

[1]State Key Laboratory of Fluid Power and Mechatronic Systems, School of Mechanical Engineering, Zhejiang University, Hangzhou 310027, China
[2]Key Laboratory of 3D Printing Process and Equipment of Zhejiang Province, School of Mechanical Engineering, Zhejiang University, Hangzhou 310027, China
[3]School of Mechanics and Safety Engineering, Zhengzhou University, Zhengzhou 450001, China
[4]Department of Biomedical Engineering, The Hong Kong Polytechnic University, Hung Hom, Kowloon, Hong Kong, China
[5]Key Laboratory of Materials Processing and Mold, Ministry of Education, Zhengzhou University, Zhengzhou 450002, China

Corresponding to Yong He, E-mail: yongqin@zju.edu.cn

Abstract

Hydrogels are very popular in biomedical areas for their extraordinary biocompatibility. However, most bio-hydrogels are too brittle to perform micro/nanofabrication. An effective method is cast molding; yet during this process, many defects occur as the excessive demolding stress damages the brittle hydrogels. Here, we propose a brand-new damage-free demolding method and a soft ultrafine fiber mold (SUFM) to replace the traditional mold. Both mechanical and finite element analysis (FEA) reveal that SUFMs have obvious advantages especially when the contact area between hydrogel and mold gets larger. By means of a high-resolution 3D printing called electrohydrodynamic (EHD) printing, SUFMs with various topological structures can be achieved with the fiber diameter ranging from 500 nm to 100 μm at a low cost. Microfluidics and cell patterns are implemented as the demonstration for potential applications. Owing to the tiny scale of microstructures and the hydrophilicity of hydrogels, significant capillary effect occurs which can be utilized to deliver liquid and cells autonomously and to seed cells into those ultrafine channels evenly. The results open up a new avenue for a wider use of hydrogels in biomedical devices, tissue engineering, microfluidics and wearable electronics; the proposed fabrication method also has the potential to become a universal technique for micro/nanofabrication of brittle materials.

Keywords: Hydrogel micro/nanofabrication, ultrafine fiber mold, damage-free demolding, micro/nano 3D printing, electrohydrodynamic printing, hydrogel bio-microfluidic chip, cell patterns

1. Introduction

Hydrogels, which are water-swollen, cross-linked hydrophilic polymer systems,[1, 2] have gained popularity in many areas like tissue engineering,[3-5] soft electronics and actuators.[6-8] For applications in tissue engineering, due to various properties including high water content similar to *in vivo* soft tissues, extraordinary biocompatibility, adjustable physicochemical properties and capability to mimic the extracellular matrix,[9, 10] hydrogels are widely used in organoids[11-14], organ on the chip,[15-18] cell pattern[19-21] and tissue regeneration.[22, 23]

A critical issue for tissue engineering is to mimic the microstructure and extracellular microenvironment in

different parts of native tissues and organs so as to facilitate specific functions of cells.[24, 25] Therefore, as hydrogels are widely used as matrix, it is important to fabricate complex hydrogel-based structures with high precision. On the one hand, additive manufacturing is an emerging approach including extrusion and light-assisted 3D printing.[26] However, it is limited to specific materials which are considered to be either printable[27] or light sensitive. Precision is another problem. For extrusion 3D printing, they can hardly produce fibers sized below 100μm due to the restriction of nozzle diameter.[28] For light-assisted 3D printing, it is also difficult for them to conduct nanofabrication. Despite techniques like two-photon polymerization (TPP) are capable of fabricating structures with a nanometer resolution,[9] their equipment is extremely expensive. On the other hand, although current micro/nanofabrication methods used in integrated circuit (IC) like lithography are mature, they are based on semiconductors,[29, 30] quartz and glasses[31, 32] which are not suitable for direct use in hydrogel manufacturing.

A most common fabrication method for hydrogel is cast molding.[15, 21, 24] During this process, molds made by IC process are utilized for casting the hydrogel precursor. After crosslinking, the hydrogel patterns are demolded and the micro/nanostructures can be obtained. However, there are several drawbacks by using this method. First of all, hydrogels with high biocompatibility are usually extremely brittle. They can be easily damaged by excessive stress when demolded from the molds. As a result, a variety of defects arise, especially when the molds have high aspect ratios, ultrafine and complex structures.[33-36] The main reason of the excessive stress in the conventional demolding method is that the contact area between the hydrogel and mold is too large. It induces a tremendous frictional force and adhesive force and then stress concentration occurs in corners of those micro/nano structures. In other words, if the contact area between the hydrogel and the mold is greatly reduced, the demolding stress will be cut down. Furthermore, it is generally accepted that cast molding, which is dependent on IC process, is costly and not efficient due to the complex procedures for fabricating molds.[37, 38] As a result, plenty of researches are devoted to looking for substitutions. The aim of our work is therefore to solve the two problems of cast molding mentioned above: 1) greatly diminish the demolding stress by reducing the contact area between the mold and the hydrogel. 2) cut down the expense and improve the fabrication efficiency.

Here, a new strategy is proposed based on the 3D printed soft ultrafine fibers as the molds (SUFMs); peeling off these fibers from the hydrogel softly leads to a damage-free demolding. Differing from conventional demolding where the contact between molds and the hydrogel is a conformal contact, there is just a tiny local contact between the fibers and the hydrogel during the damage-free demolding, which can induce significantly less adhesive and frictional force. Furthermore, bending stress generated by the deformation of hydrogel is eliminated. In other words, the damage-free demolding significantly improves the quality of demolding by reducing the demolding stress. A finite element analysis (FEA) also proved the superior performance of the damage-free demolding. Meanwhile, the EHD 3D printing[39-42] is able to print nanoscale structures. With the SUFMs fabricated by it, channels with diameters from 500nm to 100μm and patterned microstructures with a high precision can be obtained. In addition, thanks to this high resolution 3D printing method, the proposed fabrication process is not only less costly but also more efficient than traditional micro-molding. Compared with many other micro/nanofabrication methods, the damage-free demolding can easily adapt to various materials. It requires neither complex process parameters nor specific rheological property of the materials. As a result, it has the potential to become a universal technique for micro/nanofabrication of brittle materials. When it comes to the precision, our method is superior to most techniques except TPP. However, its cost is negligible compared with TPP's. Interestingly, due to the ultrafine channels and the excellent hydrophilicity of a here used hydrogel material, gelatin methacrylamide (GelMA), an obvious capillary effect can be discovered. With this effect, we could deliver liquids and even cells in the chips without extra power supplies (**Figure 1**Bi). It means that complex peripheral equipment like pumps around the traditional microfluidic chips can be abandoned.[43] As a result, we could seed cells into superfine channels with a size of only 15μm evenly and controllably, which is difficult to achieve with manual operation. Finally, by tuning the channel diameter in the chips, we could guide the cells to grow in a particular direction and even in arbitrary patterns, which demonstrates the application prospects in the fields of cell patterns (**Figure 1**Bii).

2. Results and discussion

2.1 Fabrication of 3D printed soft ultrafine fibers as the molds (SUFMs)

To obtain SUFM with a diversity of patterns and diameters, EHD 3D printing was used to deposit polycaprolactone (PCL) or other effective materials on a substrate in a predesigned printing path with high precision (**Figure 1**Ai). Then, the SUFM was framed, with the hydrogel precursor poured into the frame and cured by methods of cooling, heating or crosslinking according to the materials (**Figure 1**Aii). Finally, the SUFM was detached from the substrate along with the cured hydrogel and the fibers were peeled off from the hydrogel softly with extremely little damage; this process was called damage-free

demolding (**Figure 1**Aiii).

Figure 2 is a comparison between conventional demolding and damage-free demolding referring to their molds, process and defective forms. Templates in the conventional methods are made of hard materials like Si and quartz or comparatively soft materials like polydimethylsiloxane (PDMS). They are widely used in microelectromechanical systems (MEMS),[44] soft lithography,[45, 46] nanoimprint,[47] etc. They are all in an integral whole. As a result, when the casting material is cured, it will be restricted from all directions and bonded with the template tightly. Furthermore, the contact area between the hydrogel and the mold is the entire bottom surface, and the hydrogel needs to be completely peeled off at one sitting. This leads to an excessive friction force and adhesive force, which are proportional to the contact area.[48] Therefore, the conventional method may work when using a high strength casting material; but for the fragile hydrogel, it may not be effective especially in micro/nanofabrication where the structures with high aspect ratios and tiny scales exist.[33] Three typical defect formats are also presented, including line defects, plane defects and even a fracture.[47]

Right part of **Figure 2** is the schematic of damage-free demolding. Differing from the traditional template, the SUFM, which is composed of soft fibers and a substrate, is separable. After the curing of hydrogel, the soft fibers layer would detach from the substrate and move to the hydrogel. As a result, instead of peeling off the hydrogel from the template, it is more flexible to peel off the ultrafine and soft fibers from the hydrogel, which always has only a tiny local contact area. This generates much less friction force and adhesive force than the conventional one leading to a perfect demolding.

2.2 Mechanical analysis of two demolding process

2.2.1 Mechanism of two demolding methods. To better understand the advantage of the proposed fabrication approach, we first study the mechanism underneath. **Figure 3** provides a mechanical analysis in both microscale and macroscale view. Micro analysis only focuses on a small typical part. For conventional demolding, four key factors influence the stress condition referring to previous theories, including interface adhesive force,[49, 50] mechanical frictional force,[51, 52] bending stress and additional moment[53] (upper left part of **Figure 3**). Firstly, as the surfaces of the hydrogel and the mold are extremely close after curing, molecular interactions inevitably exist on the contact surfaces, including electrostatic force, van der Waals force and capillary force.[50] This leads to the interface adhesive force. Additionally, during the demolding process, the hydrogel and the mold have an opposite movement. With their rough surfaces, the two contact layers will drag against each other. To resist the layer deformation, they will undertake a mechanical frictional force. Similar to the molecular-mechanical theory of friction,[54] the total resistance force consists of adhesive force and mechanical frictional force. In addition, due to the elasticity of the hydrogel and the asymmetrical peeling process, deformation of the hydrogel occurs, resulting in the bending stress. Moreover, as the demolding is asymmetrical which has also been discussed by our previous work,[53] its direction cannot be vertical but has an inclined angle. The hydrogel will therefore hit against the sidewalls of the mold, which gives the hydrogel an additional moment.

By a one-by-one comparison with the four factors mentioned above, the damage-free demolding method exhibited a better performance (upper right part of **Figure 3**). Region A, which is highlighted by yellow dash lines, was extracted for analysis. Since fibers were separated from each other and could not be peeled off simultaneously, only one fiber was pulled up in the schematic. At first, the contact area between the single fiber and region A is smaller than the conventional one. As a result, the interface adhesive force is lower. Moreover, region A only suffers a unilateral mechanical frictional force which was half of the conventional one. Furthermore, during the damage-free demolding process, only the soft fiber is peeled off while the hydrogel keeps flat with no deformation. Hence, there would not be any bending stress. Finally, an inclined angle might also exist when the fiber is peeled off. Therefore, the additional moment could be similar with the conventional one. Generally, from the microscale view, damage-free demolding is superior to the conventional way.

However, microscale analysis is not comprehensive. In a real demolding process, molds have complex patterns and structures; the contact area between hydrogel and mold is at least several square centimeters. It means much more units in micro analysis are contained, which also has a big effect on the demolding quality. Accordingly, a macroscale analysis is conducted; the conventional mold and SUFM are both shown with a gridding pattern. On one hand, in the conventional method (lower left part of **Figure 3**), the whole piece of hydrogel has to be peeled off at once. Consequently, the whole bottom surface of the hydrogel interacts with the mold (shown in the internal view). The total resistant force will be the sum of all the forces and moments on every single unit in the previous micro analysis. Moreover, when the hydrogel becomes larger without adding its thickness, it will deform more easily leading to an increased bending stress. In consequence, for the conventional demolding, when the contact area increases, the resistant force and bending stress would drastically increase and defects shown in **Figure 2** would appear.

In contrast, the damage-free demolding is free from the scale effect. When peeled off from the hydrogel, the fiber has

only a local contact with the hydrogel (red circles in lower right part of **Figure 3**). Therefore, there is no significant difference for the stress condition in micro and macro situation. As a result, in macroscale, the damage-free demolding is better than conventional demolding even when the pattern is complex.

In conclusion, the damage-free demolding is superior to the conventional method from both the micro and macro perspectives.

2.2.2 Finite element analysis (FEA) of two demolding methods. To compare these two methods quantificationally, an FEA was conducted for simulation with the equivalent stress calculated. We want to investigate how the demolding stress change along with the increasing size of the hydrogel (or the increasing contact area) during these two processes. **Figure 4**Ai presents the models established to simulate the conventional demolding. On the left is a model in which a piece of hydrogel with one bulge is combined with a mold with one groove. It is regarded as a single unit with dimension shown in the diagram. Then, with its size going up, there would be more and more units in all directions. To simplify the problem, the model was only extended in the x direction and models with one, two, three, four, five and six units were adopted for further simulation. **Figure 4**Aii illustrates the change of stress during the conventional demolding process in different models (from single unit to six units). Except the curve of one unit which presents a comparatively stable trend, the other five curves show a similar tendency: they will ascend initially to the peak and then decline to zero in about 5s as a result of the hydrogel-mold detachment. The point is that the peak value increases with the growing number of units. It indicates that, in the conventional way, the maximum equivalent stress will rise when the size of the model goes up. The two inserted stress nephograms represent the stress conditions of the models with one and six units respectively at a certain time point. (see movie S1 in supplementary materials for simulation animation). Similarly, the models with single and six units to simulate damage-free demolding is demonstrated in **Figure 4**Bi. Their dimensions correspond to that of **Figure 4**Ai, but the difference is that the fibers were demolded in sequence. This resulted in a periodic stress variation and the peak values in each cycle were almost the same (**Figure 4**Bii). This is because every cycle stands for the demolding of a single fiber, which is independent of and similar to each other. Despite the increasing number of units, the maximum stress will always be at a constant level. In other words, the maximum equivalent stress will not increase too much with model sizing up. There are also two stress nephograms inserted, representing the stress conditions of the two models at a certain time point. (see movie S2 in supplementary materials for simulation animation). **Figure 4**D shows the totally different variation tendency of the maximum stress in the two methods. Initially, the maximum stress in the conventional way is already higher than that in the damage-free one. This consists with the previous micro analysis. Then the former ascends dramatically with the number of units increasing while the latter keeps stable. Especially, in the model with six units, the maximum stress in the conventional way is 23 times of that in the damage-free way within an area of only 975 μm^2. As mentioned before, it is normal for a demolding with a size of several square centimeters, which is over one million times of what we had here. In that case, the conventional demolding would have an incredibly higher stress than the damage-free way.

Compared with existing means of diminishing demolding stress including adding release agent and surface treatment of molds,[51, 55] we proposed a novel solution by decreasing the contact area between the hydrogel and mold. Furthermore, those traditional ways may introduce chemical residues which are negative to biological application while ours will not have that problem.

2.3 Micro/nano fabrication of hydrogels

To construct micro/nano channels on hydrogels with controllable size and patterns, a series of experiments were conducted to study the effects of EHD 3D printing parameters and swelling on the channel size (**Figure 5**A-E), as well as the optimal printing condition to manufacture patterned fibers and channels (**Figure 6**).

2.3.1 Effects of printing parameters and swelling on channel size. There are two printing modes used here including the melt EHD printing and solution EHD printing (**Figure 5**A). These two modes could print fibers in different diameter ranges by using different printing materials. The former could print microfibers (3-100μm) based on polymer melt. The latter could print nanofibers based on polymer solution and the finest fiber could be 500nm. Three critical fiber diameters were characterized using scanning electron microscope (SEM) containing 100μm, 3μm and 500nm (**Figure 5**Bi~Biii).

After the fibers were peeled off from the hydrogel, the initial channels were formed (**Figure 5**C). Channels' diameters equaled to the fibers' as expected. Three critical channel diameters were also characterized using SEM containing 100μm, 3μm and 500nm (**Figure 5**Ci~Ciii). Material used here was 10% (w/v) gelatin methacrylamide (GelMA, EFL-GM-60).

After the hydrogel chip with initial channels was prepared, it was seeded with cells and immersed into the culture medium. Naturally, swelling of hydrogel occurred and influenced the channel size. **Figure 5**D shows that, after about 6 h of immersion, diameters of three different channels increased by 8% (channel 1), 15% (channel 2) and 20%

(channel 3) respectively. Then, before 45h of immersion, they all continued to decrease to about 80% of the initial diameters. After 45 h of immersion, the channel diameters tended to be stable. The whole trend could be attributed to the nonuniform swelling of hydrogel, as the channels changed the geometry of the hydrogel. In summary, the swelling changed the channel size in varying degrees according to the channel diameter and the time for the channel to be stable was about 45 h.

Based on **Figure 5**A-D, experiments were designed and carried out to evaluate all effects of processing parameters on fiber diameters and channel diameters after swelling (CDAS) (**Figure 5**E). The figure shows the fiber diameters and CDAS under different printing parameters including printing speed, air pressure, and nozzle-to-substrate-distance (NSD). NSD in **Figure 5**Ei and Eii is 1 and 2mm respectively. The results indicated that the fiber diameter increased with increasing air pressure, whereas it decreased with an increasing printing speed and NSD, because the higher air pressure increased the extrusion quantity, leading to a thicker fiber. Additionally, the fiber was stretched more sufficiently by the electrostatic force and became thinner with increasing printing speed and NSD. Finally, after swelling for over 2 days, the channel size had different degrees of shrinkage (diameter decreased by 1% - 20%) when the initial diameter ranged from 20 to 100μm. However, when the initial diameter was below 20μm, the final channel size didn't change significantly.

2.3.2 Fabrication of patterned channels. In addition, the ability to fabricate channels with complex structures is imperative for mimicking the microenvironment *in vivo*. Then the subsequent scaffolds or microfluidic chips accommodate the cells well and realize specific Cellular functionalization.[25] By adjusting the printing speed to match the extrusion rate, patterned fibers were printed and the patterned channels were obtained subsequently. **Figure 6** shows three types of patterned fiber and channel with gridding-like, wave-like and eight-like structures (see SEM images of these channels in **Figure S4**).

2.4 Capillary effect of channels

Interestingly, with the outstanding hydrophilicity of GelMA (**Figure 7**A) and the channel diameter downsizing to several or hundreds of micrometers, an obvious capillary effect was discovered in the channels. With this effect, the hydrogel bio-microfluidic chips could deliver liquid autonomously without any external power supply. Although there are many capillary microfluidic chips previously, they are normally made of materials like glass which has a bad hydrophilicity or silicon and PDMS which are both hydrophobic. As a result, surface treatment must be conducted to acquire a wettable surface in advance.[56] Whereas the hydrogel-based chips do not have this problem, the hydrophilicity of hydrogels is relatively good and the contact angle of GelMA used here is below 30° (**Figure 7**A). Along with the superfine channels, hydrogel-based chips can provide sufficient capillary pressure for autonomous liquid delivery.

For further study of cell patterning, we need to seed cells inside the ultrafine channels. Normally, it is difficult to inject cell suspension into channels sized only a few or dozens of micrometers manually. The cell suspension will inevitably spill out on the whole surface of the chip inducing an uncontrollable cell density in channels and a waste of experimental materials. Therefore, a structure including an injection port (1mm in diameter) is designed (**Figure 7**B). We could easily inject cell suspension into the injection port with pipette. Then, with help of the capillary effect, cell suspension is drawn into the ultrafine channels rapidly with less leak; the cell density is more controllable by tuning the concentration of the cell suspension.

A hydrogel chip was fabricated (**Figure 7**C) to verify the feasibility of the hypothesis in **Figure 7**B. Blue dye was injected into the injection port at first. Then it flowed into channels sized 70μm quickly, demonstrating the ability of the chips to deliver liquid autonomously (please see Movie S3 in the supplementary materials). **Figure 7**D presents the capability of the chip to transport cells in a channel sized 150μm in a detailed view (please see Movie S4 in the supplementary materials). The process of delivering cells in channels sized 70μm can also be viewed in Movie S5. The delivery speed was extremely fast because of the higher flow rate in thinner channels. In other word, a controllable delivery speed could be achieved by tuning the diameter of channels, which needs a further study in the future.

Figure 7E shows a biomimetic capillary-like channel network with bilateral gradient channels sized from 200 to 30μm. This simulates some critical features found in real vascular systems, where the capillaries narrow for better waste and nutrient transport. The confluence of red and blue dye solutions in the network verifies the interconnection and good performance of the chip (please see Movie S6 in the supplementary materials). Significantly, this structure can be used for making functionalized vessel-on-a-chip with a high precision,[15, 18] which is vital for 3D cell culture, disease modeling and drug screening.

2.5 Biocompatibility of the hydrogel bio-microfluidic chip

To evaluate the biocompatibility of the hydrogel bio-microfluidic chip, two types of cells including human skin fibroblasts (HSFBs) and human umbilical cord vein endothelial cells (HUVECs) were seeded into the channels sized 100 μm uniformly by the method mentioned above. The material used here was 10% GelMA with a Young's modulus about 10Kpa. **Figure 8**A shows that both kinds of

cells adhered to the channels since day 1 and kept proliferating throughout the 7-day culture. The relative optical densities (OD) of samples was in a gradual rising trend indicating a normal proliferation rate (**Figure 8**B). Comparing these two types of cells, HUVECs had a higher proliferation rate. Cell viability was counted on days 1, 4 and 7 showing high viabilities of >98% at different culture times for both cell types (**Figure 8**C). As a result, the chips based on GelMA had a good biocompatibility.

Figure 8D shows the morphology and distribution of the two types of cells in the channels after the 7-day culture. Both types of cells didn't grow out of the channels, though channels had been filled with cells. It indicated that the channels could restrict the cellular activity in a specific region and might even guide the growth of cells in particular orientation. The reason could be that the surface roughness in and out of the channels were different or the cells were just trapped in the channels due to the depth.

2.6 Analysis of cell orientation

To further verify the capability of channels to guide the cell growth in particular directions, quantitative research should be conducted to study the conditions that would make this phenomenon happen. The hypothesis was that reducing the channel size to a degree would force most cells to grow along the direction of the channel. As a result, the variable chosen here was channel diameter, ranging from 15-150μm (**Figure 9**A). In this experiment, HSFBs were chosen because of its slender morphology which was easier for recognizing its direction. Corresponding to **Figure 9**A, chips with channels sized 15, 30, 90 and 150μm were fabricated. Then, HSFBs were seeded into these channels and cultured for 7 days. **Figure 9**B shows a series of confocal images of the samples displaying different levels of cell orientation in different channels. With the channels downsizing, cell orientation became more obvious which verified the hypothesis. When the channels' diameter reached 15μm (~ cell diameter), even single HSFB were restrained by the channel tightly as shown in **Figure 9**Biv. The alignment of the HSFBs in channels was further analyzed by quantifying the angles between single cells and the axis of channels (**Figure 9**C). An angle equal to 90° indicates perpendicularly alignment of the cells, while an angle of 0° represents a perfect alignment along the channel axis. Cells were considered aligned when the angle was below 20°. Increasing the channel diameter significantly decreased the degree of orientation from 100% ± 0 (15μm), 98% ± 2.8% (30μm), 71% ± 8% (90μm) to 50% ± 11.7% (150μm) ($P<0.001$). As expected, channels sized 150μm exhibited an almost uniform distribution of the angles referred to unoriented cell growth. In contrast, alignment angles in channels sized 15μm were all below 10° indicating a highly oriented cell growth. In conclusion, the bio-microfluidic chips can be applied for cell orientation by tuning channel diameters on it. Accordingly, a cell-like patterned channel network was fabricated and seeded with HUVECs. Finally, the cells grew and filled this network forming a cell-like shape which proved the capability to guide cell orientation (**Figure S5**). Based on the facts above, we hypothesize that the underlying mechanism of the cell orientation and elongation is a combined effect of the geometric confinement and the cell response to the stress (mainly the compressive stress) from the external environment. Similar phenomenon about cell orientation have also been reported before and were investigated both theoretically and experimentally.[57-60] Peter et al.[57] pointed out that The mechanical stresses, including compression, frictional shear and tension, could alter the structural properties of cells to make them adapt to a sustained mechanical environment. Since the cells were tightly restricted by the sidewalls of the channels, they have to change their shape to balance the intracellular tension with the external stress. Furthermore, Jeremiah et al.[59] demonstrated that endothelial cells, under a pure compression, would realign perpendicular to the compressing direction. The compression can affect other parts of the cell like ion channels, focal adhesion, microtubules, cell membrane and might trigger the release of certain substances and signals influencing the cell orientation. A similar research conducted by Bonnie et al.,[60] which utilized microchannels to study cell shape and function, showed the elongation and orientation of endothelial cells with the channel width decreasing. It consists with our results and concludes that this phenomenon is not only a simple geometric confinement but also the reaction of the endothelial cells to the side walls and cell-cell signaling. The compression of the side walls initially induced the change of the cell shape and orientation. Our hypothesis could be validated preliminarily according to the researches above while a further experimental verification, which is beyond the scope of the present study, could be conducted in the future. This fantastic function has the potential for building neural network *in vitro* by guiding the growth of nerve cells.[61, 62] It also provides a powerful tool for studying mechanism of cell behaviors.[63] Furthermore, multi rows of channels with specific spacing can be used to form many kinds of tissues like skin and myocardial tissue.[21, 64, 65]

3. Conclusions

In summary, a strategy based on SUFM and then peeling off these fibers from hydrogels is proposed to fabricate hydrogel bio-microfluidic chips, which is called damage-free demolding. It exhibits an extraordinary performance compared with the conventional way according to the mechanical and FEA analysis, where the maximum equivalent stress of the conventional demolding was about 23 times of that in the damage-free demolding within an area

of only 975 μm^2. It is predictable that, with the growing size of the contact area, the difference between these two methods will become massive. Due to the high precision of the EHD printing and the damage-free demolding, micro/nano channels ranging from 500nm to 100μm can be manufactured on the fragile hydrogels. Patterned and biomimetic microstructures can also be made. Capillary effect discovered in the chips were fully used to deliver liquid and cells autonomously and cells could be seeded into those ultrafine channels evenly. Finally, a biological application for cell orientation was also realized on the chips by tuning diameters of single channel. We believe that the damage-free demolding presented here can improve the micro-molding technology greatly to fulfill the requirements of hydrogel-based micro/nanofabrication. The hydrogel bio-microfluidic chip made here can provide a good platform for capillary microfluidics, organ-on-the-chip, cell pattern, tissue regeneration, etc.

4. Experimental Section

4.1 Materials preparation

PCL (CAPA6800, Perstorp Ltd, Sweden) was used to fabricate the SUFMs by the method of melt EHD printing. Its molecular weight is 80,000g/mol and the melting temperature is 60℃.

20% (w/v) PCL solution was used to fabricate the SUFMs by the method of solution EHD printing. It was prepared by dissolving PCL in glacial acetic acid (99.5%, Shanghai Macklin Biochemical Co., Ltd, Shang Hai, China).

The hydrogel used here for casting is 10% (w/v) GelMA (Suzhou Intelligent Manufacturing Research Institute, Suzhou, China). It was prepared by dissolving GelMA (EFL-GM-60) in MEM (Tangpu Biological Technology Co., Ltd., Hangzhou, China) containing 0.5% (w/v) lithium phenyl-2, 4, 6- trimethylbenzoylphosphinate (LAP) for 3h.

4.2 EHD 3D printing device and parameters

A direct writing device (EFL-MDW5800, Suzhou Intelligent Manufacturing Research Institute, Suzhou, China) was used to deposit PCL for fabricating the sacrificial layers. The device consisted of motorized XYZ stages, a nozzle, two heaters to heat the PCL polymer, a high voltage generator and a pneumatic system to adjust the extrusion pressure. Two printing modes were implemented on this device, including melt EHD printing and solution EHD printing. For the former one, the temperature of the two heaters was set to 70 ℃ for the heater of nozzle (inner diameter 350μm) and 75 ℃ for the heater of syringe. Air pressure supplied to the polymer melt was 7.5, 15 and 25kPa. Additionally, the print speed was set from 20 to 100mm/min when nozzle-to-substrate-distance (NSD) was 1mm with a voltage of 3.3kV. When NSD was 2mm, it was set from 500 to 2500mm/min with a voltage of 4.7kV. For the solution EHD printing, heaters were not required. The inner diameter of the nozzle was 90μm. The printing speed was 4000mm/min with an NSD of 0.5mm and voltage of 1.5kV. For printing fibers with complex patterns, the NSD was 1 mm with a printing speed from 5-20mm/min and an air pressure of 7.5kPa.

4.3 Characterization of channels in the bio-microfluidic chips

To characterize the channels with different diameters, a SEM system was utilized which is described in section 4.5.

To characterize different formations of microchannel networks, channels with straight, waved and eight-shaped structures were loaded with fluorescent microbead suspension (0.1% w/v); then, they were imaged by a confocal fluorescence microscope (OLYMPUS FV3000).

Variation of channel diameter induced by swelling: To investigate the variation of channel diameter due to the swelling of hydrogel after immersing the chips in the culture medium, three types of hydrogel chips with channels in different sizes (300, 400 and 650μm) on them were made. The material used here was 10% (w/v) GelMA (EFL-GM-60) and the culture medium was the same as the one used in section 4.6 The channel sizes were measured at 0.5, 1.5, 2.5, 4, 6, 8, 10, 12, 24, 46, 68h after the chips were put into culture medium at 37℃.

4.4 Characterization of capillary effect

The material used to fabricate the chips was 10% (w/v) GelMA (EFL-GM-60).

To characterize the capillary effect, the channels were injected with red and blue dye (Kaiguilai Co., Ltd., Shanghai, China). The whole process was observed and recorded in real time using a digital camera (Nikon D810) with microlens (AF-S MICRO Nikkor 105mm 1:2.8G ED, Nikon).

To characterize the transportation of cells in channels using the capillary effect, the channels were injected with the prepared cell suspension. The whole process was recorded in brightfield using an inverted optical microscope (OLYMPUS CKX41).

4.5 Scanning Electron Microscopy Analysis

In this study, an SEM system (SU-6600, Hitachi, Tokyo, Japan) was used for SEM analysis. A sputter coater (Ion Sputter E-1045, Hitachi, Tokyo, Japan) was used to coat samples with platinum before imaging.

For samples without cells. To characterize the channels with different diameters, the samples were freeze dried at first. Then they were coated in the sputter coater and imaged in the SEM system. To observe the morphology of the fibers printed by EHD printing, samples were directly coated in the

sputter coater and then imaged in the SEM system.

For samples with cells. Firstly, the samples were fixed with 4% paraformaldehyde (Solarbio Co., Ltd., Shanghai, China) for more than 4 h at room temperature. Then for dehydration, the samples were soaked in a series of ethanol solutions (30%, 50%, 70%, 80%, 90%, 95%, and 100%) for 30 min respectively. After that, the samples were critical-point dried. Finally, they were coated with platinum and imaged in the SEM system.

4.6 Cell culture and seeding cells into channels

HUVECs and HSFBs were cultured in ECM (Qizhenhu Biological Technology Co., Ltd., HangZhou, China) with 10% fetal bovine serum (Qizhenhu Biological Technology Co., Ltd., HangZhou, China), 1% penicillin (100 units/mL), and streptomycin (100μg/mL) (Qizhenhu Biological Technology Co., Ltd., Hang Zhou, China) at 37℃ in 5% CO2. The culture medium was changed every two days. Both types of cells were passaged using trypsin-EDTA (Tangpu Biological Technology Co., Ltd., Hangzhou, China) dissociation, when they reached around 90% confluence. Culture flasks with 90% cell confluency were washed with phosphate-buffered saline (PBS) (Qizhenhu Biological Technology Co., Ltd., Hangzhou, China) and incubated with 0.25% trypsin-EDTA for 1-3 min at 37 ℃ in 5% CO2 to detach the culture flasks. After that, the cell suspension was centrifuged at 1000rpm for 5 min at room temperature and the supernatant was discarded. Finally, the cells were resuspended in the cell culture medium to a concentration of 10M cells mL-1.

To seed those two kinds of cells into ultrafine channels with diameter below 100μm, injection ports with larger diameters were designed and set beside the ultrafine channels. First, the prepared cell suspension was loaded into the injection ports. Then, with the help of capillary effect, the cell suspension was driven into the ultrafine channels. After 3 h of cell attachment, the whole pieces of cell-laden hydrogel chips were immersed in fresh culture medium and cultured statically with the medium changed every other day. Finally, they were cultured for several days before characterizations.

4.7 Cell viability Analysis

The cell viability was analyzed using a cell LIVE/DEAD assay. First, the cell-laden hydrogel chips were washed with PBS for 3 times before staining. Then, the samples were stained with LIVE/DEAD assay reagents (Key-GEN BioTECH Co., Ltd., Nanjing, China) according to the manufacturer's instructions. Calcein AM and propidium iodide (PI) were diluted with PBS to a concentration of 2 and 8 μM, respectively. After an incubation in the Calcein AM/PI mixture for 30 min in the dark, the samples were washed with PBS to remove residual reagents. Lastly, the cell-laden hydrogel chips were imaged by acquiring two images in each frame under a confocal fluorescence microscope (OLYMPUS FV3000). Red and green were for live and dead cells, respectively.

4.8 Cell proliferation Analysis

Cell proliferation was tested using a cell counting Kit-8 (CCK-8; Dojindo Chemical Technology Co., Ltd., Shanghai, China). The cell-laden hydrogel chips were cultured in culture dishes separately for 1,4 and 7 days. First of all, the culture medium was removed, and the samples were moved to a 24-well plate. Then they were washed with PBS for three times. After that, a mixture of 1450μL of MEM and 50μL of CCK- 8 reagent was added to each well. Finally, after 3 hours of incubation, the solutions were transferred to a 96-well plate to measure the optical density (OD) values at a wavelength of 450nm.

4.9 Cell morphology Analysis

Morphologies of HUVECs and HSFBs were visualized by cell cytoskeleton staining which included F-actin and nucleus staining. Referring to the kit instructions, the F-actin and nucleus were stained using TRITC phalloidin (Yeasen Biological Technology Co., Ltd., Shanghai, China) and 2-(4-amidinophenyl)-6-indolecarbamidine dihydrochloride (DAPI) staining solution (Yeasen Biological Technology Co., Ltd., Shanghai, China). First, the samples were washed in PBS and fixed with 4% paraformaldehyde for 30 min. After that, the samples were washed with PBS again and permeabilized with 0.5% Triton X-100 (Solarbio Co., Ltd., Shanghai, China) for 5 min. Subsequently, they were washed with PBS and stained with TRITC phalloidin (0.1μM) for 30 min in the dark. Next, they were washed with PBS and stained with DAPI (10μg/mL) for 10 min in the dark. Finally, the samples were wash with PBS for the last time and imaged using a confocal fluorescence microscope (OLYMPUS FV3000).

4.10 Simulations for FEA

The ANSYS software (ANSYS Inc., USA) was employed to simulate the two demolding processes and a series of models with different units (from one to six) were established. The hyperelastic material model was used to simulate the hydrogel while both the fibers in damage-free demolding and the mold in conventional demolding were based on silicon material for controlling variables.

4.11 Statistical analysis

Data is presented as mean ± standard deviation of independent replicates. Statistical analysis is conducted using ANOVA, and statistical significance was determined at $p < 0.05$.

Acknowledgements

The authors would like to acknowledge the Testing Center in Su Zhou Intelligent Manufacturing Research Institute for providing SEM and confocal testing. This work was sponsored by the National Key Research and Development Program of China (2018YFA0703000), the National Nature Science Foundation of China (No. 51622510, U1609207, 51375440, 11702233), the Science Fund for Creative Research Groups of National Natural Science Foundation of China (No. 51821093), the Nature Science Foundation of Zhejiang Province, China (No. LR17E050001), the Fundamental Research Funds for the Central Universities, and the Key Research and Development Program of Zhejiang Province (No. 2017C01063).

References

[1] Zhang Y S,Khademhosseini A 2017 Advances in engineering hydrogels *Science* **356** eaaf3627.
[2] Zhu J,Marchant R E 2011 Design properties of hydrogel tissue-engineering scaffolds *Expert Review of Medical Devices* **8** 607-26.
[3] Billiet T,Vandenhaute M,Schelfhout J,Van Vlierberghe S,Dubruel P 2012 A review of trends and limitations in hydrogel-rapid prototyping for tissue engineering *Biomaterials.* **33** 6020-41.
[4] Ansari M,Eshghanmalek M 2019 Biomaterials for repair and regeneration of the cartilage tissue *Bio-Design and Manufacturing* **2** 41-49.
[5] Saroia J,Yanen W,Wei Q,Zhang K,Lu T,Zhang B 2018 A review on biocompatibility nature of hydrogels with 3D printing techniques, tissue engineering application and its future prospective *Bio-Design and Manufacturing* **1** 265-79.
[6] Lin S,Yuk H,Zhang T,Parada G A,Koo H,Yu C,Zhao X 2016 Stretchable Hydrogel Electronics and Devices *Adv. Mater.* **28** 4497-505.
[7] Jeong K-U,Jang J-H,Kim D-Y,Nah C,Lee J H,Lee M-H,Sun H-J,Wang C-L,Cheng S Z D,Thomas E L 2011 Three-dimensional actuators transformed from the programmed two-dimensional structures via bending, twisting and folding mechanisms *J. Mater. Chem.* **21** 6824-30.
[8] Wang E,Desai M S,Lee S-W 2013 Light-Controlled Graphene-Elastin Composite Hydrogel Actuators *Nano Letters* **13** 2826-30.
[9] You S,Li J,Zhu W,Yu C,Mei D,Chen S 2018 Nanoscale 3D printing of hydrogels for cellular tissue engineering *Journal of Materials Chemistry B* **6** 2187-97.
[10] Drury J L,Mooney D J 2003 Hydrogels for tissue engineering: scaffold design variables and applications *Biomaterials.* **24** 4337-51.
[11] Schneeberger K,Spee B,Costa P,Sachs N,Clevers H,Malda J 2017 Converging biofabrication and organoid technologies: the next frontier in hepatic and intestinal tissue engineering? *Biofabrication* **9** 013001.
[12] Chang R,Emami K,Wu H,Sun W 2010 Biofabrication of a three-dimensional liver micro-organ as anin vitrodrug metabolism model *Biofabrication* **2** 045004.
[13] Ma X,Qu X,Zhu W,Li Y-S,Yuan S,Zhang H,Liu J,Wang P,Lai C S E,Zanella F,Feng G-S,Sheikh F,Chien S,Chen S 2016 Deterministically patterned biomimetic human iPSC-derived hepatic model via rapid 3D bioprinting *Proceedings of the National Academy of Sciences* **113** 2206-11.
[14] Zhao H,Chen Y,Shao L,Xie M,Nie J,Qiu J,Zhao P,Ramezani H,Fu J,Ouyang H,He Y 2018 Airflow-Assisted 3D Bioprinting of Human Heterogeneous Microspheroidal Organoids with Microfluidic Nozzle *Small* **14** 1802630.
[15] Nie J,Gao Q,Wang Y,Zeng J,Zhao H,Sun Y,Shen J,Ramezani H,Fu Z,Liu Z,Xiang M,Fu J,Zhao P,Chen W,He Y 2018 Vessel-on-a-chip with Hydrogel-based Microfluidics *Small* **14** 1802368.
[16] Lee S-A,No D Y,Kang E,Ju J,Kim D-S,Lee S-H 2013 Spheroid-based three-dimensional liver-on-a-chip to investigate hepatocyte–hepatic stellate cell interactions and flow effects *Lab on a Chip* **13** 3529-37.
[17] Huh D,Matthews B D,Mammoto A,Montoya-Zavala M,Hsin H Y,Ingber D E 2010 Reconstituting Organ-Level Lung Functions on a Chip *Science* **328** 1662-68.
[18] Nie J,Gao Q,Xie C,Lv S,Qiu J,Liu Y,Guo M,Guo R,Fu J,He Y 2019 Construction of multi-scale vascular chips and modelling of the interaction between tumours and blood vessels *Materials Horizons*.
[19] Théry M,Racine V,Piel M,Pépin A,Dimitrov A,Chen Y,Sibarita J-B,Bornens M 2006 Anisotropy of cell adhesive microenvironment governs cell internal organization and orientation of polarity *Proceedings of the National Academy of Sciences* **103** 19771-76.
[20] Waterkotte B,Bally F,Nikolov P M,Waldbaur A,Rapp B E,Truckenmüller R,Lahann J,Schmitz K,Giselbrecht S 2014 Biofunctional Micropatterning of Thermoformed 3D Substrates *Adv. Funct. Mater.* **24** 442-50.
[21] Rim N G,Yih A,Hsi P,Wang Y,Zhang Y,Wong J Y 2018 Micropatterned cell sheets as structural building blocks for biomimetic vascular patches *Biomaterials.* **181** 126-39.
[22] Zhao X,Lang Q,Yildirimer L,Lin Z Y,Cui W,Annabi N,Ng K W,Dokmeci M R,Ghaemmaghami A M,Khademhosseini A 2016 Photocrosslinkable Gelatin Hydrogel for Epidermal Tissue Engineering *Advanced Healthcare Materials* **5** 108-18.
[23] Sun X,Zhao X,Zhao L,Li Q,D'Ortenzio M,Nguyen B,Xu X,Wen Y 2015 Development of a hybrid gelatin hydrogel platform for tissue engineering and protein delivery applications *Journal of Materials Chemistry B* **3** 6368-76.
[24] Zorlutuna P,Annabi N,Camci-Unal G,Nikkhah M,Cha J M,Nichol J W,Manbachi A,Bae H,Chen S,Khademhosseini A 2012 Microfabricated Biomaterials for Engineering 3D Tissues *Adv. Mater.* **24** 1782-804.
[25] Schober A,Fernekorn U,Singh S,Schlingloff G,Gebinoga M,Hampl J,Williamson A 2013 Mimicking the biological world: Methods for the 3D structuring of artificial cellular environments *Engineering in Life Sciences* **13** 352-67.
[26] He Y,Wu Y,Fu J-z,Gao Q,Qiu J-j 2016 Developments of 3D Printing Microfluidics and Applications in Chemistry and Biology: a Review *Electroanal.* **28** 1658-78.
[27] He Y,Yang F,Zhao H,Gao Q,Xia B,Fu J 2016 Research on the printability of hydrogels in 3D bioprinting *Scientific Reports* **6** 29977.
[28] Mandrycky C,Wang Z,Kim K,Kim D-H 2016 3D bioprinting for engineering complex tissues *Biotechnol. Adv.* **34** 422-34.
[29] Henning A K,Fitch J S,Harris J M,Dehan E B,Cozad B A,Christel L,Fathi Y,Hopkins D A,Lilly L J,McCulley W,Weber W A,Zdeblick M 1998 Microfluidic MEMS for semiconductor processing *IEEE Transactions on Components, Packaging, and Manufacturing Technology: Part B* **21** 329-37.
[30] Friis P,Hoppe K,Leistiko O,Mogensen K B,Hübner J,Kutter J P 2001 Monolithic integration of microfluidic channels and optical waveguides in silicaon silicon *Appl. Optics.* **40** 6246-51.
[31] Rodriguez I,Spicar-Mihalic P,Kuyper C L,Fiorini G S,Chiu D T 2003 Rapid prototyping of glass microchannels *Anal. Chim. Acta*

496 205-15.
[32] Bu M,Melvin T,Ensell G J,Wilkinson J S,Evans A G R 2004 A new masking technology for deep glass etching and its microfluidic application *Sensors and Actuators A: Physical* **115** 476-82.
[33] Müller E,Pompe T,Freudenberg U,Werner C 2017 Solvent-Assisted Micromolding of Biohybrid Hydrogels to Maintain Human Hematopoietic Stem and Progenitor Cells Ex Vivo *Adv. Mater.* **29** 1703489.
[34] Tang M D,Golden A P,Tien J 2004 Fabrication of Collagen Gels That Contain Patterned, Micrometer-Scale Cavities *Adv. Mater.* **16** 1345-48.
[35] Golden A P,Tien J 2007 Fabrication of microfluidic hydrogels using molded gelatin as a sacrificial element *Lab on a Chip* **7** 720-25.
[36] Takehara H,Nagaoka A,Noguchi J,Akagi T,Sakai T,Chung U-i,Kasai H,Ichiki T 2013 Implementation of tetra-poly(ethylene glycol) hydrogel with high mechanical strength into microfluidic device technology *Biomicrofluidics* **7** 054109.
[37] Urrios A,Parra-Cabrera C,Bhattacharjee N,Gonzalez-Suarez A M,Rigat-Brugarolas L G,Nallapatti U,Samitier J,DeForest C A,Posas F,Garcia-Cordero J L,Folch A 2016 3D-printing of transparent bio-microfluidic devices in PEG-DA *Lab on a Chip* **16** 2287-94.
[38] Chen C,Mehl B T,Munshi A S,Townsend A D,Spence D M,Martin R S 2016 3D-printed microfluidic devices: fabrication, advantages and limitations—a mini review *Analytical Methods* **8** 6005-12.
[39] Sun D,Chang C,Li S,Lin L 2006 Near-Field Electrospinning *Nano Letters* **6** 839-42.
[40] Wang X,Zheng G,Xu L,Cheng W,Xu B,Huang Y,Sun D 2012 Fabrication of nanochannels via near-field electrospinning *Applied Physics A* **108** 825-28.
[41] Xie C,Gao Q,Wang P,Shao L,Yuan H,Fu J,Chen W,He Y 2019 Structure-induced cell growth by 3D printing of heterogeneous scaffolds with ultrafine fibers *Mater. Design.* **181** 108092.
[42] Brown T D,Dalton P D,Hutmacher D W 2011 Direct Writing By Way of Melt Electrospinning *Adv. Mater.* **23** 5651-57.
[43] Olanrewaju A,Beaugrand M,Yafia M,Juncker D 2018 Capillary microfluidics in microchannels: from microfluidic networks to capillaric circuits *Lab on a Chip* **18** 2323-47.
[44] Wang G J,Chen C L,Hsu S H,Chiang Y L 2005 Bio-MEMS fabricated artificial capillaries for tissue engineering *Microsyst. Technol.* **12** 120-27.
[45] Annabi N,Tsang K,Mithieux S M,Nikkhah M,Ameri A,Khademhosseini A,Weiss A S 2013 Highly Elastic Micropatterned Hydrogel for Engineering Functional Cardiac Tissue *Adv. Funct. Mater.* **23** 4950-59.
[46] Karp J M,Yeh J,Eng G,Fukuda J,Blumling J,Suh K-Y,Cheng J,Mahdavi A,Borenstein J,Langer R,Khademhosseini A 2007 Controlling size, shape and homogeneity of embryoid bodies using poly(ethylene glycol) microwells *Lab on a Chip* **7** 786-94.
[47] Jiang W,Ding Y,Liu H,Lu B,Shi Y,Shao J,Yin L 2008 Two-Step curing method for demoulding in UV nanoimprint lithography *Microelectron. Eng.* **85** 458-64.
[48] Guo Y,Liu G,Xiong Y,Tian Y 2006 Study of the demolding process—implications for thermal stress, adhesion and friction control *J. Micromech. Microeng* **17** 9-19.
[49] Pollock H M,Maugis D,Barquins M 1978 The force of adhesion between solid surfaces in contact *Appl. Phys. Lett.* **33** 798-99.
[50] Komvopoulos K,Yan W 1997 A Fractal Analysis of Stiction in Microelectromechanical Systems *Journal of Tribology* **119** 391-400.
[51] Guo Y,Liu G,Zhu X,Tian Y 2007 Analysis of the demolding forces during hot embossing *Microsyst. Technol.* **13** 411-15.
[52] Peng Z,Gang L,Yangchao T,Xuehong T 2005 The properties of demoulding of Ni and Ni-PTFE moulding inserts *Sensors and Actuators A: Physical* **118** 338-41.
[53] He Y,Fu J-Z,Chen Z-C 2007 Research on optimization of the hot embossing process *J. Micromech. Microeng* **17** 2420-25.
[54] Zhang X,Zhang Y,Wang J,Sheng C,Li Z 2018 Prediction of Sliding Friction Coefficient Based on a Novel Hybrid Molecular-Mechanical Model *Journal of Nanoscience and Nanotechnology* **18** 5551-57.
[55] Choi W M,Park O O 2003 A soft-imprint technique for direct fabrication of submicron scale patterns using a surface-modified PDMS mold *Microelectron. Eng.* **70** 131-36.
[56] Olanrewaju A O,Robillard A,Dagher M,Juncker D 2016 Autonomous microfluidic capillaric circuits replicated from 3D-printed molds *Lab on a Chip* **16** 3804-14.
[57] Davies P F,Tripathi S C 1993 Mechanical stress mechanisms and the cell. An endothelial paradigm *Circ. Res.* **72** 239-45.
[58] Nestor-Bergmann A,Goddard G,Woolner S,Jensen O E 2017 Relating cell shape and mechanical stress in a spatially disordered epithelium using a vertex-based model *Mathematical Medicine and Biology: A Journal of the IMA* **35** i1-i27.
[59] Wille J J,Ambrosi C M,Yin F C-P 2004 Comparison of the Effects of Cyclic Stretching and Compression on Endothelial Cell Morphological Responses *Journal of Biomechanical Engineering* **126** 545-51.
[60] Gray B L,Lieu D K,Collins S D,Smith R L,Barakat A I 2002 Microchannel Platform for the Study of Endothelial Cell Shape and Function *Biomedical Microdevices* **4** 9-16.
[61] Taylor A M,Blurton-Jones M,Rhee S W,Cribbs D H,Cotman C W,Jeon N L 2005 A microfluidic culture platform for CNS axonal injury, regeneration and transport *Nature Methods* **2** 599-605.
[62] Park J W,Vahidi B,Taylor A M,Rhee S W,Jeon N L 2006 Microfluidic culture platform for neuroscience research *Nature Protocols* **1** 2128-36.
[63] Wang M,Cheng B,Yang Y,Liu H,Huang G,Han L,Li F,Xu F 2019 Microchannel Stiffness and Confinement Jointly Induce the Mesenchymal-Amoeboid Transition of Cancer Cell Migration *Nano Letters*.
[64] Sun Y,Jallerat Q,Szymanski J M,Feinberg A W 2014 Conformal nanopatterning of extracellular matrix proteins onto topographically complex surfaces *Nature Methods* **12** 134.
[65] Lind J U,Busbee T A,Valentine A D,Pasqualini F S,Yuan H,Yadid M,Park S-J,Kotikian A,Nesmith A P,Campbell P H,Vlassak J J,Lewis J A,Parker K K 2016 Instrumented cardiac microphysiological devices via multimaterial three-dimensional printing *Nature Materials* **16** 303.

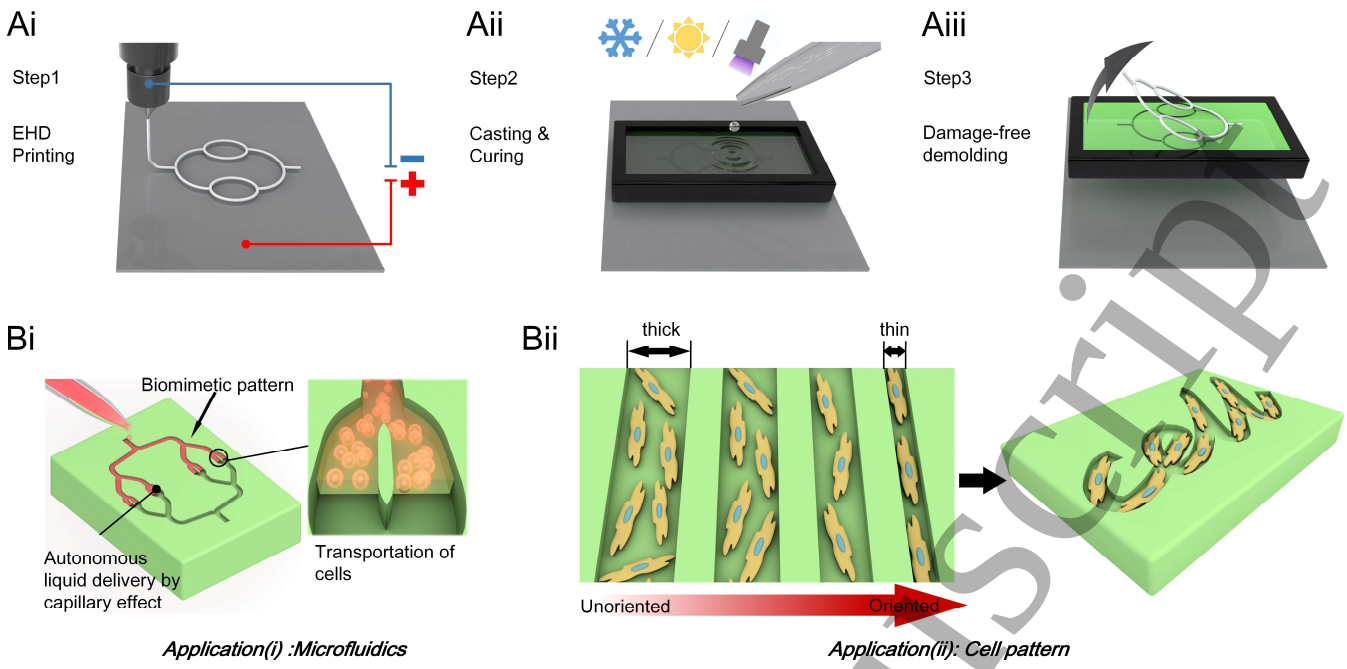

Figure 1. Fabrication of the hydrogel bio-microfluidic chip and the two applications. (A) Fabrication process: (i) 3D printed SUFM through EHD 3D printing. (ii) Casting and curing the hydrogel precursor. Curing methods: cooling, heating, crosslinking, etc., according to the materials. (iii) Obtaining the bio-microfluidic chip by peeling off the fibers on the hydrogel (damage-free demolding). (B) Sketch of two applications of the hydrogel bio-microfluidic chip. (i) Microfluidics with capillary effect which can deliver liquid and cells autonomously. (ii) Cell pattern: cells grow in a certain direction by tuning the channel diameter and can be patterned by predefined channels.

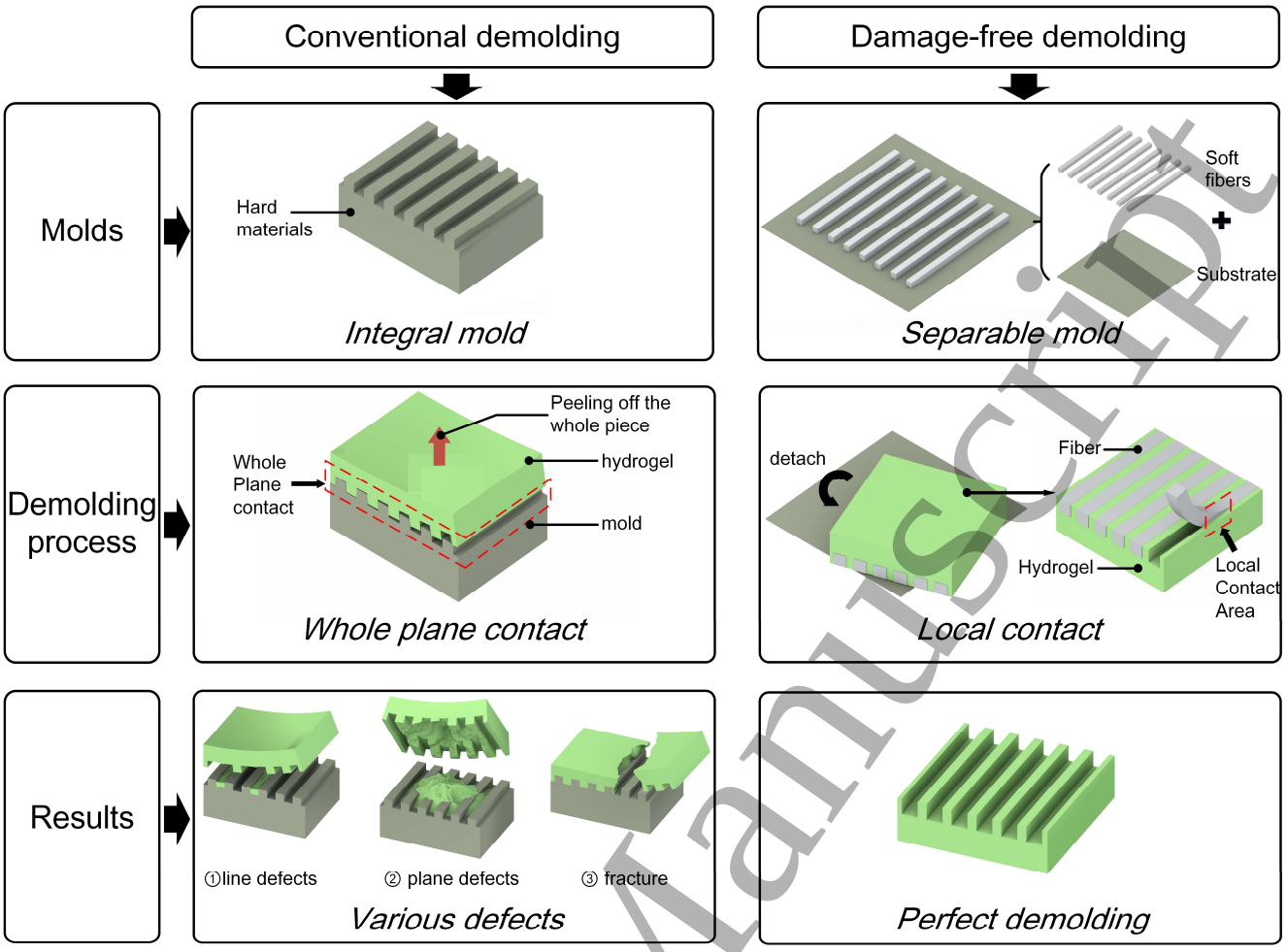

Figure 2. Preliminary comparison of damage-free demolding and the conventional one with respect to molds, demolding process and quality of demolding.

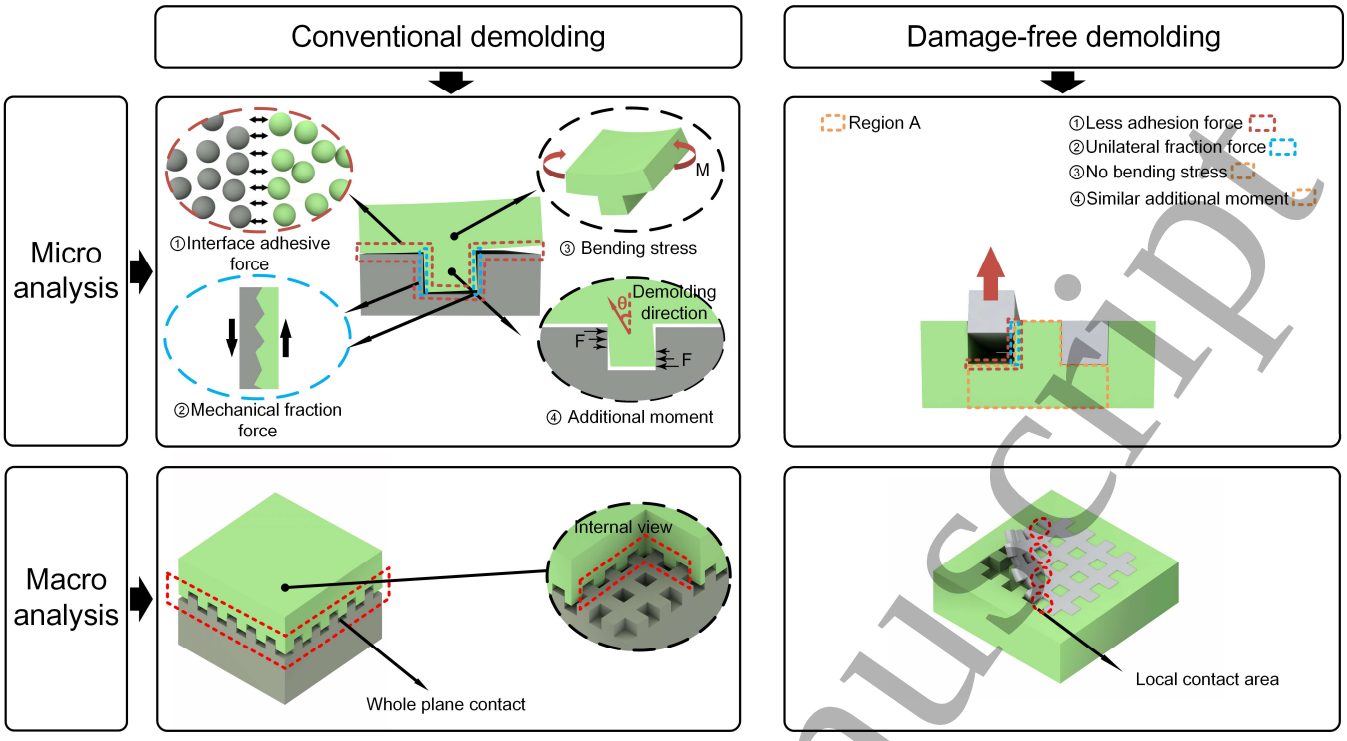

Figure 3. Mechanical analysis of two demolding processes including the micro and macro analysis of the conventional demolding and damage-free demolding.

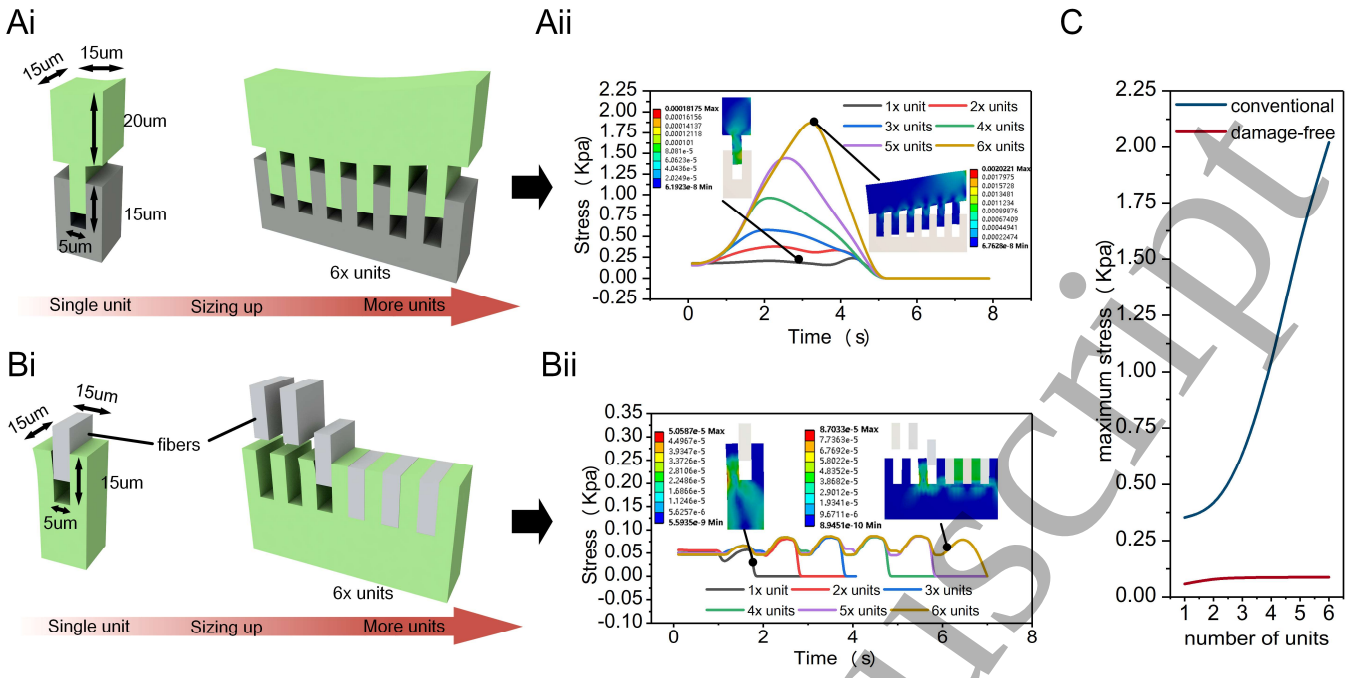

Figure 4. (A) Finite element analysis of conventional demolding: (i) Illustration of simulation models (ii) Variation of stress during the demolding process in models with different sizes (from one unit to six units). (B) Finite element analysis of damage-free demolding: (i) Illustration of simulation models (ii) Variation of stress during the demolding process in models with different sizes (from one unit to six units). (C) Maximum stress of the two methods changing with the number of units in the models.

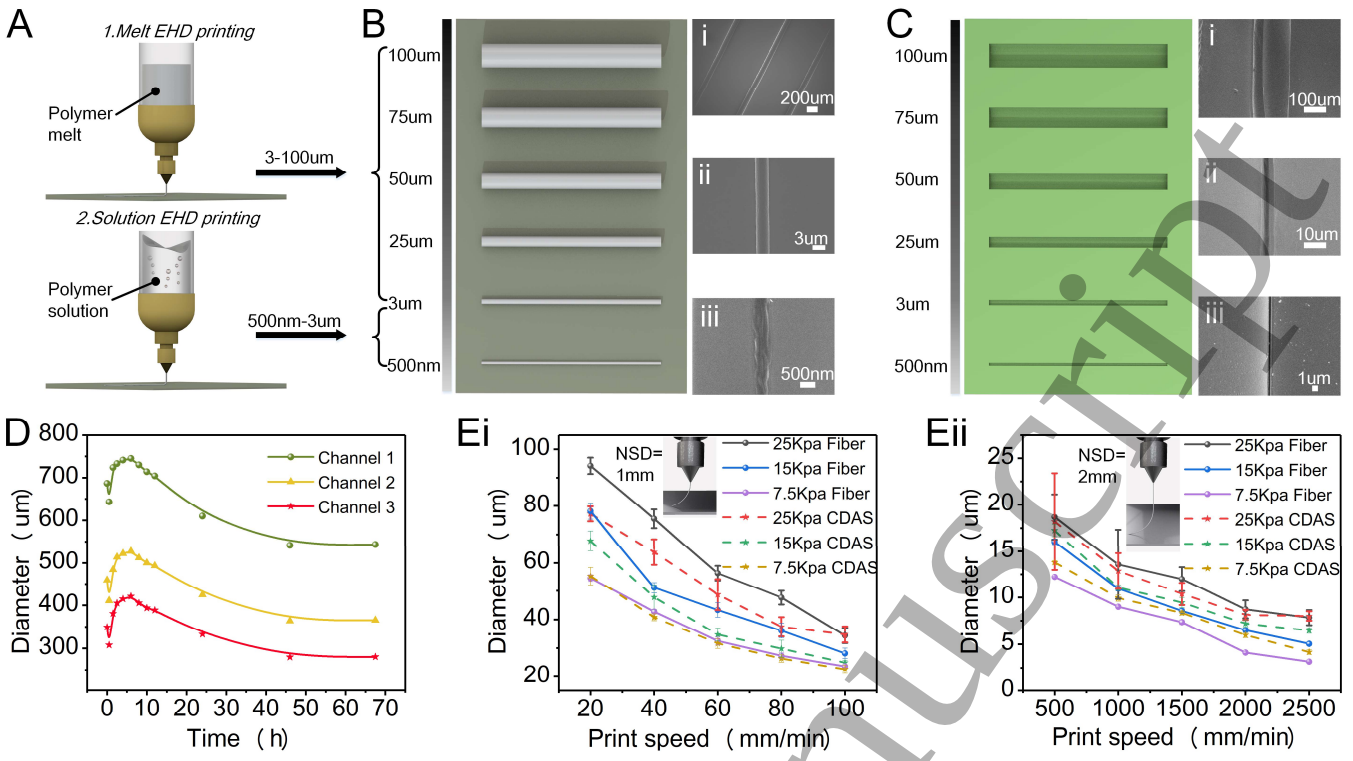

Figure 5. Characterization of the fabrication process. (A) Sketch of two modes of EHD 3D printing for different ranges of fiber diameter from 500nm to 100μm, including melt EHD printing and solution EHD printing. (B) Range of the initial the fiber diameter: (i)~(iii) SEM images of fibers with diameters of 100μm, 3μm and 500nm. (C) Range of the initial channel diameter after demolding corresponding to the fiber diameter in (B). (i)~(iii) SEM images of channels with diameters of 100μm, 3μm and 500nm. (D) Diameter change of three channels in different sizes due to the swelling after immersion in the culture medium. (E) The effect of the printing parameters on the fiber diameter and channel diameter after swelling (CDAS). (i) NSD =1 mm for fiber diameters from 20-100μm. (ii) NSD =2 mm for fiber diameters from 3-20μm. (data is presented as mean value ± standard deviation of independent replicates)

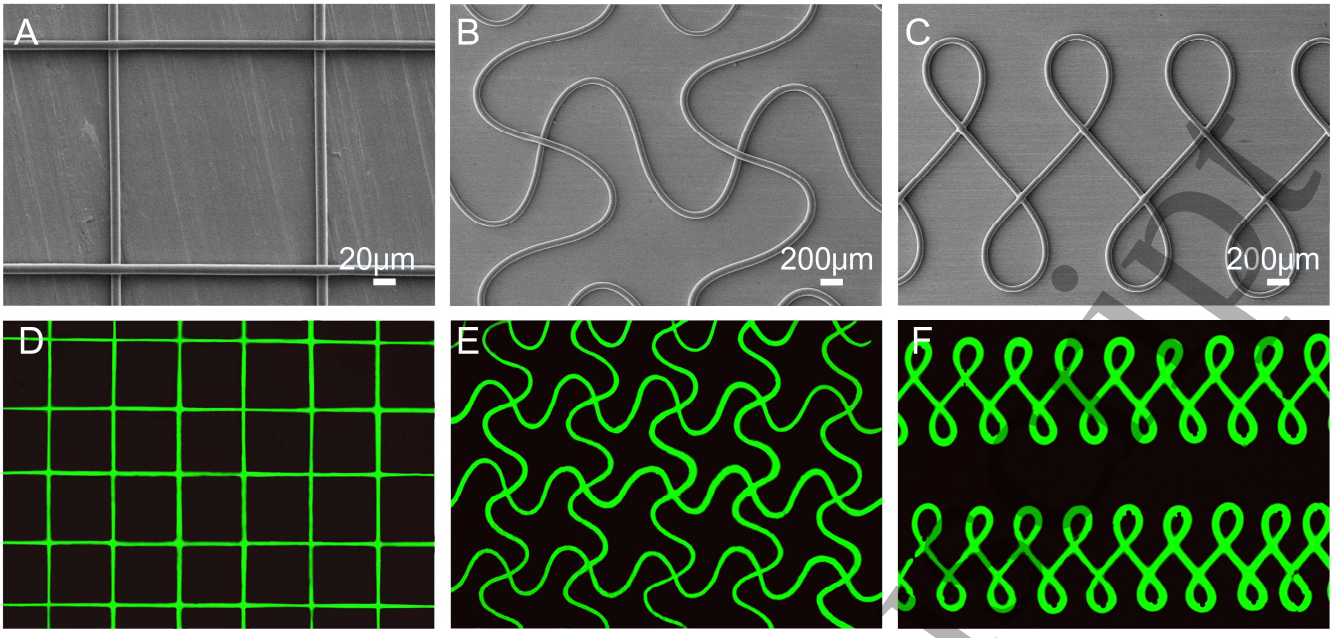

Figure 6. Different patterned fibers and channels. (A)~(C) SEM images of different patterned fibers with gridding-like, wave-like and eight-like structures. (D)~(F) Fluorescent images of different patterned channels corresponding to (A)~(C).

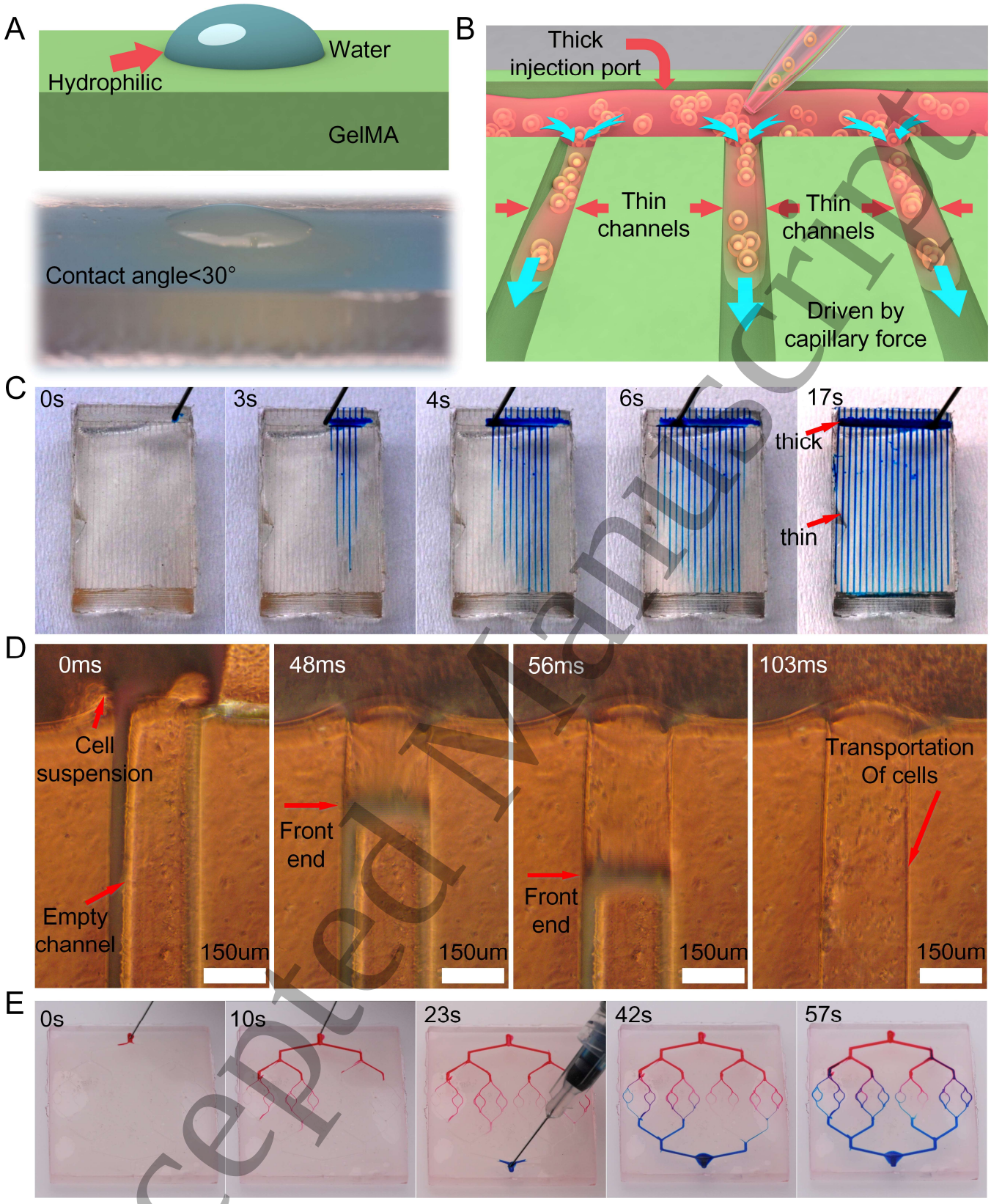

Figure 7. Capillary effect of the bio-microfluidic chip. (A) Hydrophilicity of GelMA. (B) Sketch of the transportation of cells in the bio-microfluidic chip using the capillary force. (C) Sequential images within 17 s of perfusions showing the fluid flow from the injection port to the channels. (D) Sequential images within 103ms showing the use of capillary effect to transport

cells. (E) Sequential images within 57s of perfusions showing the fluid flows through the entire capillary-like channel network. Red and blue dye solutions were dropped at two sides respectively, and merged in the center.

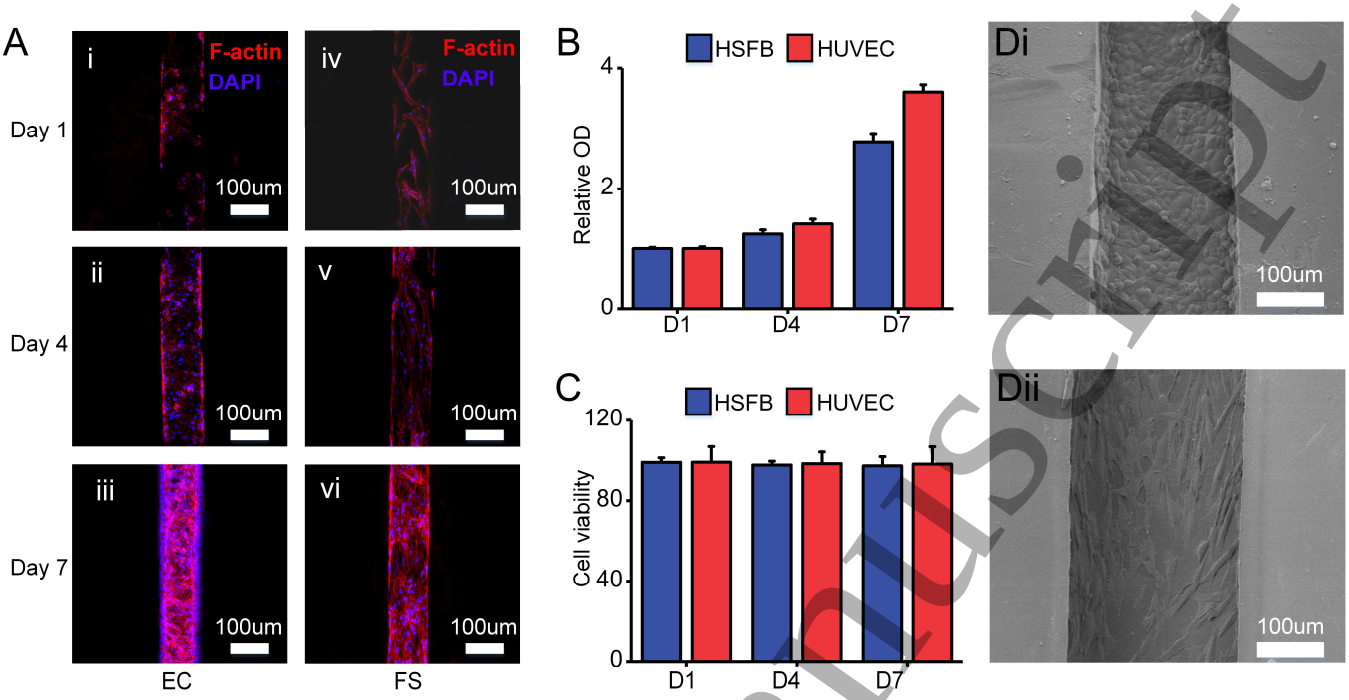

Figure 8. Characterization of cell growth in the channels. (A) Confocal images of cytoskeleton staining of 100μm channels with HSFBs and HUVECs in it. (i)~(iii) Confocal images of HUVECs in the channel after 1, 2 and 7 days of static culture. (iv)~(vi) Confocal images of HSFBs in the channel after 1, 2 and 7 days of static culture. (B) Cell proliferation rate of HSFBs and HUVECs seeded in the channels. (data is presented as mean value ± standard deviation of independent replicates) (C) Viability of the HSFBs and HUVECs seeded in the channels. (data is presented as mean value ± standard deviation of independent replicates) (Di) SEM image of a 100μm channel with HUVECs in it after 7 days of culture. (Dii) SEM image of a 100 μm channel with HSFBs in it after 7 days of culture.

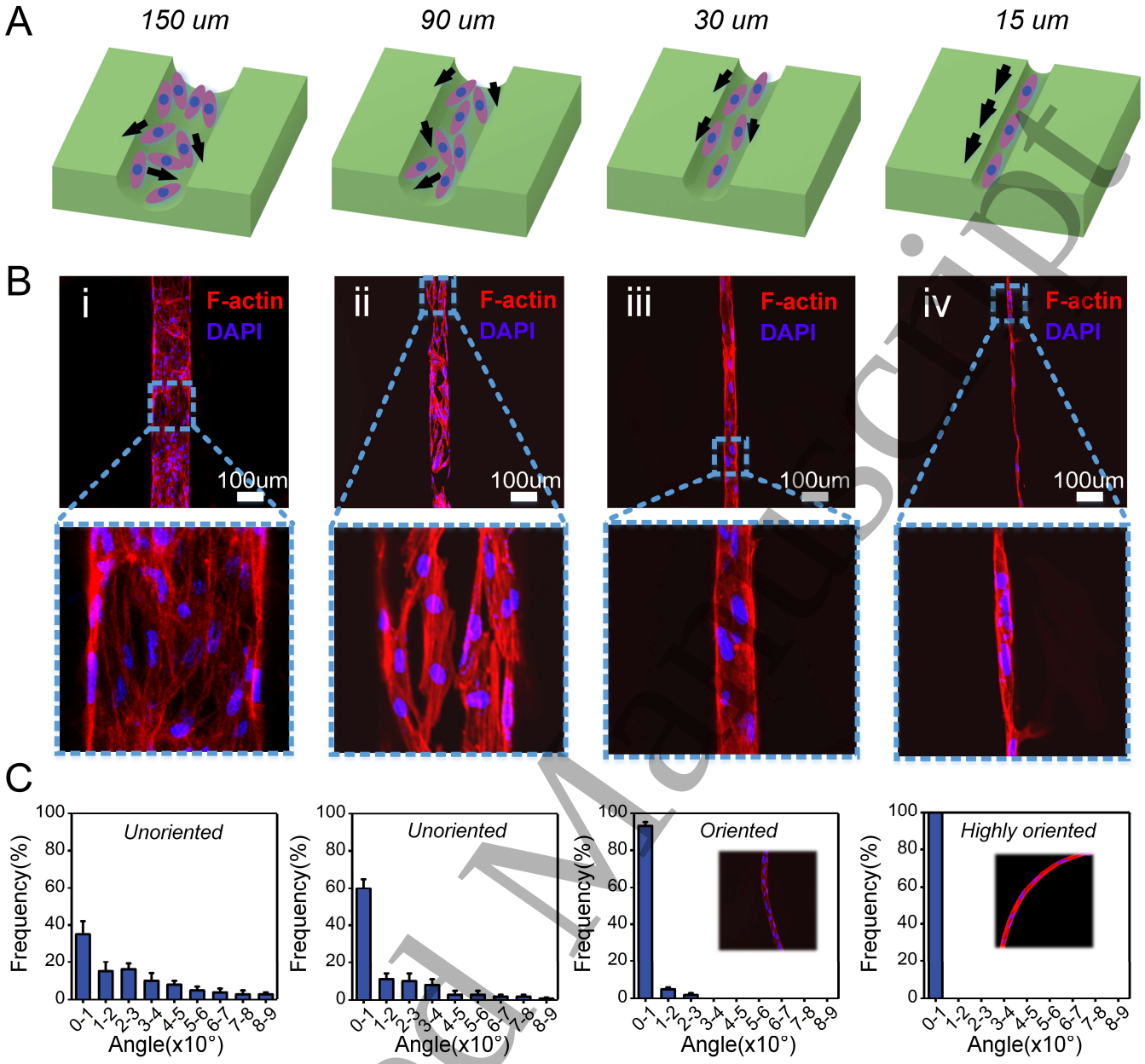

Figure 9. Effect of the channel diameter on the cell orientation. (A) Sketch of different degrees of cell orientation in different channels with diameters of 15, 30, 90 and 150μm. (Bi)~(Biv) Representative confocal images of HSFBs in the channels with diameters of 15, 30, 90 and 150μm, showing varying degrees of cell orientation. Lower panels: partial enlarged images of the upper ones, showing the detailed cell alignment. (C) Quantification of the angle distribution of HSFBs in the four types of channels. Insets are confocal images of the oriented and highly oriented HSFBs (data is presented as mean value ± standard deviation of independent replicates).